ARMY RESEARCH LABORATORY

Spatially Resolved Combustion Species and Temperatures of Solid Propellant Flames Using Snapshot Spectroscopy

by Barrie E. Homan
and John A. Vanderhoff

ARL-TR-2060 October 1999

The findings in this report are not to be construed as an official Department of the Army position unless so designated by other authorized documents.

Citation of manufacturer's or trade names does not constitute an official endorsement or approval of the use thereof.

Destroy this report when it is no longer needed. Do not return it to the originator.

Abstract

Experimental improvements have been made in the ultraviolet (UV)-visible absorption spectroscopy technique applied to propellant flame diagnostics. The two-dimensional (2-D) feature of an intensified charge-coupled device (ICCD) detector was used to simultaneously record multiple, spatially distinct absorption spectra over a region of 0.35 cm. Temporal resolution has been increased to 1 ms by pulsing a simmering xenon arc lamp. The resulting increase in the light intensity by 30 to 70 times over the nonpulsed output provides the necessary light flux to achieve single-pulse, multiple absorption spectra. Species with low concentrations can be measured with the inclusion of multiple-pass optics to increase the effective path length through the combustion region. Due to broadband UV-visible absorption observed in propellant flame spectra, only 20% of the incident light is typically transmitted. However, inclusion of a calibrated neutral density filter during the measurement of the incident intensity (I_0) allows the dynamic range of the detector to be effectively increased by a factor of 5. With these improvements, temperature and OH and NO concentration maps, with 1-ms temporal resolution, have been determined for two different propellant flames.

Table of Contents

INTENTIONALLY LEFT BLANK.

List of Figures

INTENTIONALLY LEFT BLANK.

List of Tables

INTENTIONALLY LEFT BLANK.

1. Introduction

Flames from solid propellant combustion can display up to three distinct gaseous phases at low to medium pressures: the fizz zone, or primary flame zone; dark zone; and luminous flame. The sizes of these zones depend not only on pressure but also on propellant composition. At low pressures, near the deflagration limit, many propellants do not display the final luminous flame. With an increase of pressure, a luminous flame is established at a standoff distance from the surface. This standoff region includes the fizz zone and dark zone. Low-vulnerability (LOVA) nitramine propellants, of which XM39* is an example, burn poorly at low pressures. The dark zone of these propellants exhibits pronounced temporal variation, where, at one moment, the dark zone region appears one-dimensional (1-D) with a well-defined flame standoff and, at the next moment, part of the luminous flame attaches to the burning surface [1]. Because of these effects, several modifications have been introduced into the absorption experiment.

In the past, absorption spectroscopy has been used successfully to measure both absolute concentrations and temperatures in solid propellant flames [1–7]. Because absorption is directly related to absolute concentration and temperature, it has an advantage over other nonintrusive in-situ measurement techniques. Due to quenching effects and signal collection geometry considerations, laser-induced fluorescence (LIF) cannot easily give absolute concentrations directly. Usually, such measurements are calibrated with absorption spectroscopy to convert relative concentration to an absolute scale [6]. Previous absorption measurements increased the signal-to-noise ratio (S/N) by collecting multiple, long exposures. Spatial information was gathered by changing the physical height of the probing beam with respect to the sample surface. This technique must assume that the flame maintains a steady-state condition over extended periods of time. Two pictures, captured 0.033 s apart, of XM39 propellant burning in 1.6 MPa N_2 are shown in Figures 1 and 2. The pronounced temporal variation in the flame structure

*Composition of XM39: RDX, 76%; cellulose acetate butyrate, 12%; nitrocellulose (NC) (12.6% nitrogen), 4%; acetyl triethel citrate, 7.6%; ethyl centralite, 0.4%.

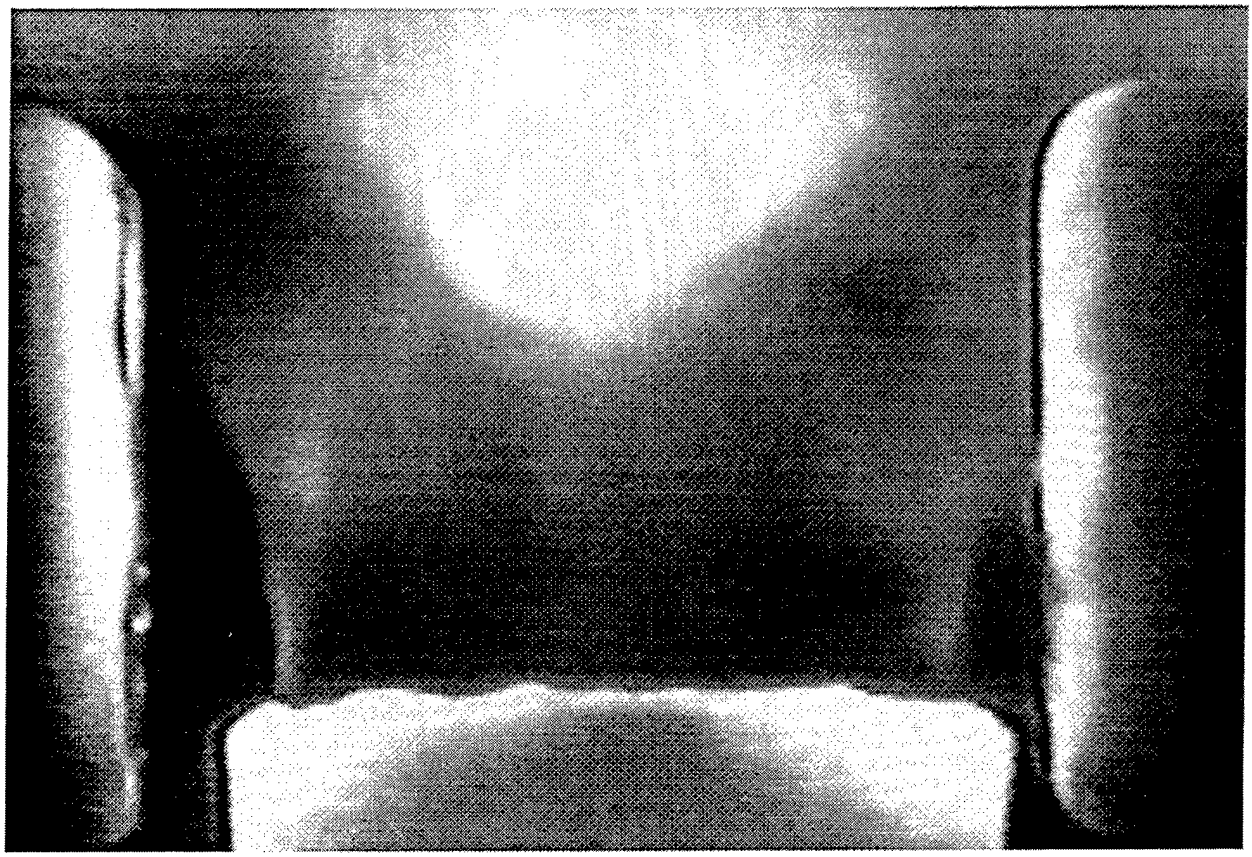

Figure 1. Photo of XM39 Burning in 1.6 MPa of N_2 (One Frame Before Data Collection Pulse).

highlights the need to measure these parameters simultaneously in height, with a shorter time resolution.

Snapshot absorption results for XM39 and JA2* compared with literature values are reported in this paper. Both propellants have been extensively studied in the literature [2–6] and are used to validate the experimental procedure. As minor species like CN and NH have mole fractions (MFs) on the order of 100 ppm, inclusion of triple-pass optics facilitates the measurements of these trace combustion components [8].

*Composition of JA2: NC (13.04% nitrogen), 58.2%; NG, 15.8%; diethylene glycol dinitrate, 25.2%; akardit II, 0.74%; magnesium oxide, 0.05%; graphite, 0.03%.

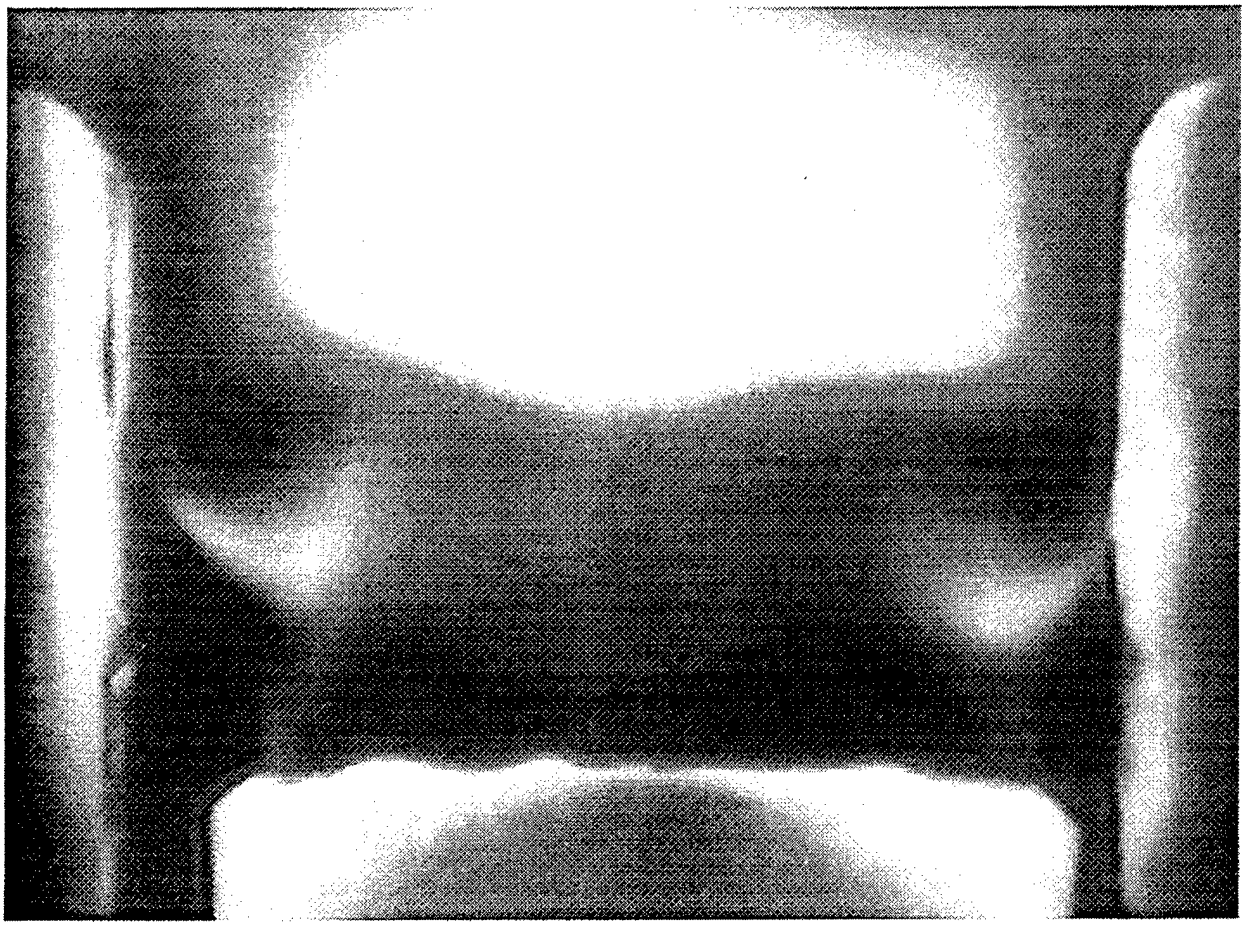

Figure 2. Photo of XM39 Frame During Data Collection.

2. Experimental/Data Analysis

The experimental setup is shown in Figure 3, where the light source consists of one of two possible xenon arc lamps contained in an Oriel housing. For NO spectroscopy in the ultraviolet (UV) region with a wavelength shorter than 250 nm, a Suprasil envelope lamp (Osram XBO 150 w/4) is used, whereas a standard quartz envelope lamp (ORC XM-150-hs) is substituted for longer wavelengths needed for OH spectroscopy. To eliminate the need to provide pulses in the kilovolt range to strike the arc, the lamps are initially started and kept simmering. A low-voltage pulse can then be easily added to the operating lamp. Pulsing is accomplished by capacitive discharge using the circuit [9] shown in Figure 4. This circuit is composed of trigger input,

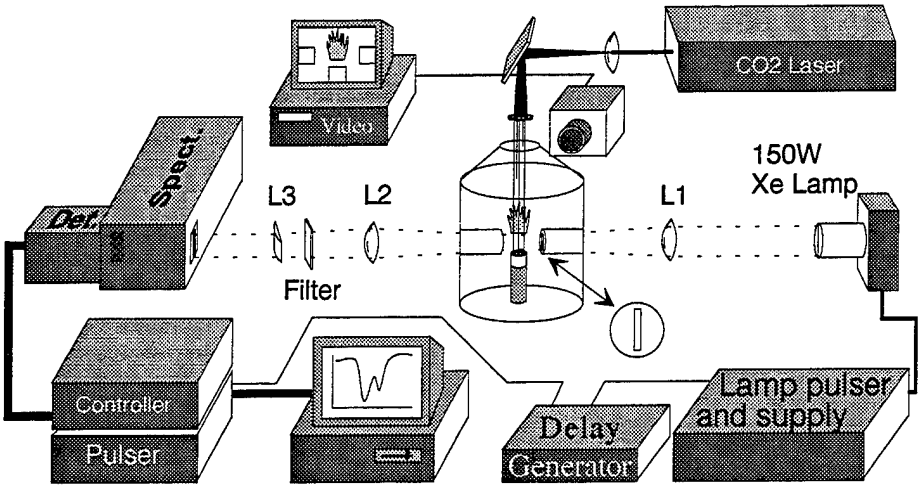

Figure 3. Experimental Apparatus.

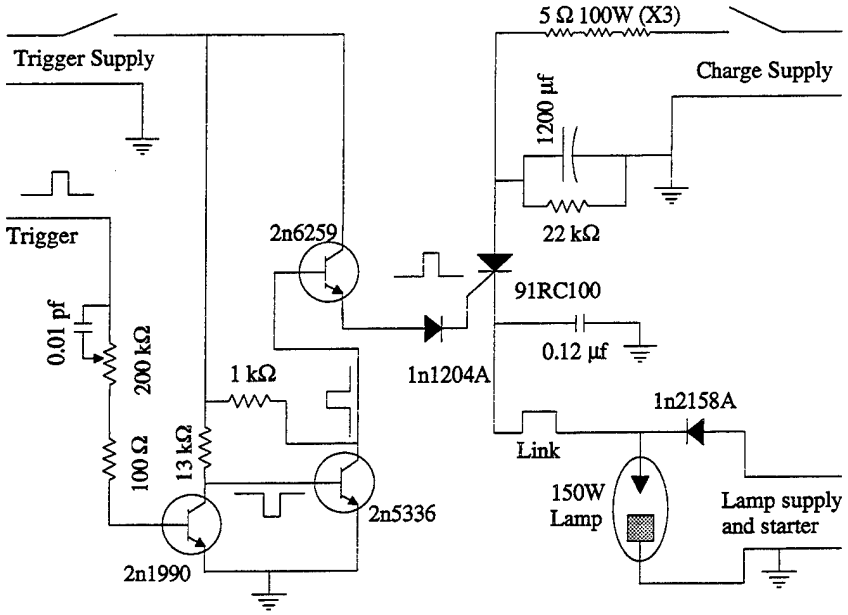

Figure 4. Pulsing Circuit.

charging, and simmering sections. Any direct-current (DC) offset from the transistor-to-transistor logic (TTL) compatible input signal is removed by the input capacitor and variable resistor. The trigger is then amplified by the two power transistors before passing to the Silicon Controlled Rectifier (SCR IR 71RC80A). A 1,200-µf capacitor, used as the pulse source, is charged with a current-limited, 0–250-V, 120-mA power supply. Here, the pulse

energy can range from 0.25 to 2 J, depending on the intensity output needed. The tradeoff for higher light output is decreased lamp life. The lamp supply and starter are standard Oriel components (Model C-72-20). To prevent damage to the pulsing electronics, the link is removed when the lamp is started. The lamp current is then adjusted to a minimum value that provides lamp stability. In the reference on which this circuit is based [9], the author was able to provide a 20-Hz output. Depending on the energy needed, the circuit reported here can operate between 4 (high energy) and 12 (low energy) pulses per second. The problem lies with turning off the SCR. To provide the reverse voltage to shut off the SCR, the lamp supply must be able to recover faster than the charging supply. The 450-W xenon lamp used in the reference with its associated larger lamp supply can recover faster than the present 150-W supply.

The source light is collected from the arc by a condenser built into the lamp housing. This light is further focused to a minimum at the sample position by a quartz spherical lens (L1 in Figure 3). To maximize the intensity at the sample, a compromise must be made between the magnification of the light source system and the solid angle collected by the lens. For a given set of optics, the intensity at the sample position will depend on the arc size, with the smaller arc having the advantage. The 150-W lamp was chosen for its small arc size. Light enters and exits the pressure chamber through 1.5- × 8-mm vertical slits, covered with sapphire windows, that define the dimensions of the light sheet. These slits are mounted on snouts that extend into the chamber, reducing the absorption path length outside the combustion region. For minor species measurements [8], the end faces can be angled and part of the sapphire windows is made reflective by aluminum evaporation (see Figure 5). The resulting multiple-pass arrangement increases the effective path length by a factor close to 3. Upon exiting the chamber, the light is collected and the line is focused onto the spectrometer slits with spherical (L2) and cylindrical (L3) lenses, respectively. The range and resolution for the simultaneously measured individual spectra are adjusted by changing the distance between L2 and the sample (and subsequently changing the distance between the sample and the detector), effectively changing the magnification. A bandpass filter of the proper wavelength is included to eliminate signal from wavelengths outside the region of interest.

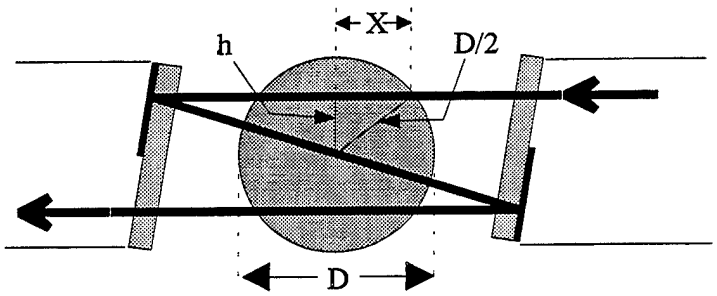

Figure 5. Triple-Pass Optics (Path Length [PL] = D + X = D + $((D/2)^2 - h^2)^{1/2}$).

The propellant sample was ignited by means of a 25-W CO_2 laser (Synrad Model D48-2). This beam is focused to a 2-mm spot in the center of the sample through a ZnSe window on top of the chamber. This ignition spot size covered 18–33% of the propellant end face, depending on the sample size used. The propellant would tend to burn from the center outward in a cupped fashion. To minimize this effect, the tops of the samples were shaved into a cone shape to closely match the ignition source. Acquisition of a higher power CO_2 laser (Synrad Model 57-1, 100 W) eliminated the need for the cone. To produce a uniform ignition profile, the far-field beam pattern was used by extending the beam path to 600 cm. The required use of three copper mirrors reduced the power delivered to the sample by over 50%. The final configuration removes 2 of the mirrors and inserts a ZnSe multifaceted optic (H in Figure 3), producing 16 evenly spaced ignition points over 75% of the sample surface.

Over these wavelength regions, the intensity measured at the detector is adjusted by either changing the pulse voltage applied to the lamp or by adjusting the gain of the detector. Increases in intensity are accomplished by increasing the pulse voltage, whereas decreasing the gain can improve the signal/noise. In Figure 6 the ratio of the pulsed-to-nonpulsed output represents the improvement in light intensity by the pulsing technique. Light pulses of 0.75 ms (full width at half maximum [FWHM]) were recorded with a detector, gated on for a duration of 1 ms. In the nonpulsed mode, the arc lamp was operated at its standard current for continuous wave (cw) output and, again, the detector gated on for a 1-ms time duration. Using a charging voltage of 50 V on the capacitor, an increase of 20–25 times the light intensity over the non-pulsed mode is observed. Increasing the charging voltage to 75 V results in a magnitude increase of about 60

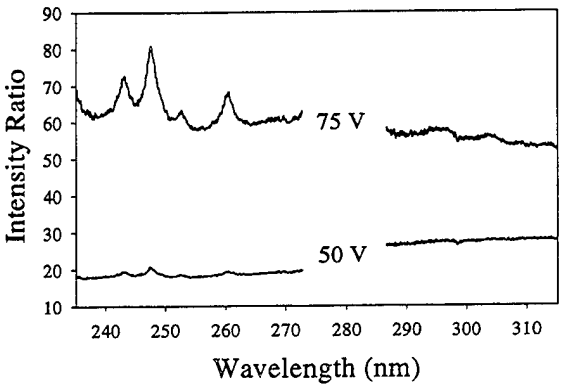

Figure 6. Effect of Pulse Voltage on Lamp Output (Ratio of Pulsed to Nonpulsed Output).

times. Much of the work reported here is in the UV (235–315nm) portion of the spectrum, where the NO and OH species absorb light. Concentrations of NO in the dark zone of propellant flames are sufficiently large to cause 100% absorption in the (0,0) ground-state transition at 226 nm. Thus, meaningful measurements for this set of circumstances are obtained from the (0,1) and (0,2) transitions around 236 and 247 nm, respectively.

Wavelength dispersion is accomplished with an Acton Research Co. SpectraPro 275 imaging spectrometer with a focal length of 0.275 m and entrance slits of 0.050 mm. Three gratings (3,600, 1,200, and 600 grooves/mm) are available via keyboard selection. The detector is a Princeton Instruments 578- × 384-pixel (0.024 mm square), thermoelectrically cooled, intensified charge-coupled device (ICCD) and is only sensitive to light upon application of a gate pulse to the microchannel plate intensifier. This feature allows short exposures to be controlled by a pulser timed to coincide with the light pulse of the xenon lamp. The 14-bit analog-to-digital (A/D) converter for the detector controller limits the dynamic range of the detector to less than 16,383 counts. In some wavelength regions, there exists broad background absorption, possibly due to scattering from large molecules or particulates [10]. This background can attenuate the transmission by as much as 80%, with a corresponding reduction in signal dynamic range. Maintaining the transmitted light intensity during combustion (I) near the detector saturation point by increasing the light source output, would greatly exceed the detector limits in the measurement of intensity before combustion event (I_0). To compensate, a neutral-density (nd)

filter of an appropriate known value can be placed in the beam during measurement of I_0. The modified transmission in this case is calculated by

$$T = \frac{I - B}{10^{\alpha} I_0 - B}, \tag{1}$$

where α is the nd filter value and B is the background spectrum taken with the light blocked from entering the spectrometer.

The CCD is divided into strips in which adjacent pixels in the spatial direction are binned together in hardware. These strips are collected by a binning capacitor that has a dynamic range of only twice that of an individual pixel. In addition, the software will only allow 10 bins to be visually displayed at one time in separate windows. Therefore, the first setup consisted of 10 bins of 38 strips each (4 strips were ignored). Subsequently, an increase in the S/N was accomplished by reducing the number of strips binned in hardware to four, while simultaneously increasing the intensity of the light to near saturation levels. These bins were then summed postprocess in software to create 12 spectra. The price paid for the S/N increase was in the collection speed, as the time it takes to read out the CCD chip is given by

$$T_R = n \times 5.8\,\text{ms/strip} + 62.524\,\text{ms}, \tag{2}$$

where n is the number of strips read. Increasing n from 10 to 96 increased the readout time by 400%, thereby reducing the frame collection frequency to $\approx$ 1.5 Hz. Therefore, the overall data collection frequency becomes limited by the detector readout time. The spatial range and resolution of the system is determined by a razorblade attached to a translational stage and positioned at the sample. The detector was set up to sum in hardware and read 10 strips corresponding to 10 of the 12 strips used to collect data. The height of the razor is then adjusted for each strip until half maximum in intensity is reached. Therefore, the position of the stage corresponds directly to the height of each bin. The amount of crosstalk between channels was

estimated by looking at the amount of signal in an adjacent covered strip during the calibration. This value is quite small (5–10%) and includes stray light not directly contributing to the absorption measurement. The last two bins are calculated from the linear fit of the calibration. The calibration of bin height for these experiments is shown in Figure 7. The resolution of the system in this case is 0.3310 mm, with a spatial range of 3.97 mm. This calibration is for the strips summed in software. Each of these bins is made up of eight smaller sub-bins, with spatial resolution of 0.041 mm.

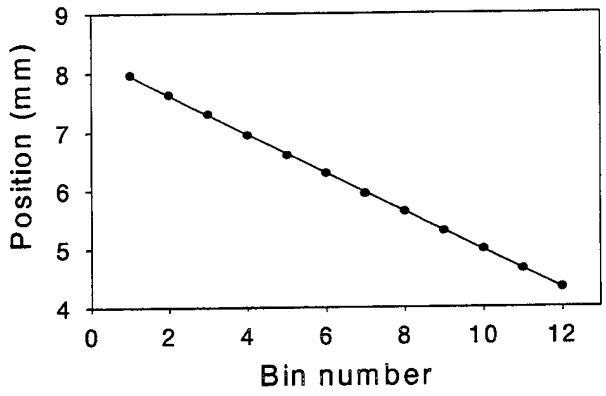

Figure 7. Spatial Calibration: Position of Razor Blade vs. Bin Number (● = Data, — = Linear Fit, Slope = -0.3310 mm/bin, r^2 = 0.999).

From each of the aforementioned strips, an intensity profile is obtained (Figure 8). These profiles are then converted to transmissions by the use of equation (1) to produce transmission spectra. The spectra are then fitted using a nonlinear, least-squares program [2] to obtain best values for temperature and concentration. This program is capable of fitting a linear background, linear or nonlinear wavelength calibration [11], as well as temperature and molecular concentration. The nonlinear wavelength technique was used when fitting the more highly wavelength-resolved OH absorption spectra. The linear wavelength technique proved adequate for the lower resolution NO measurements shown in Figure 8. For linear wavelength calibration, the emission from a spectral calibration pen lamp [Oriel Hg(Ne) 6035] is collected to provide the wavelength-per-channel calibration used in the fitting routine. As there is a slight variation in the wavelength offset between strips, this parameter is allowed to float. There are no measurable

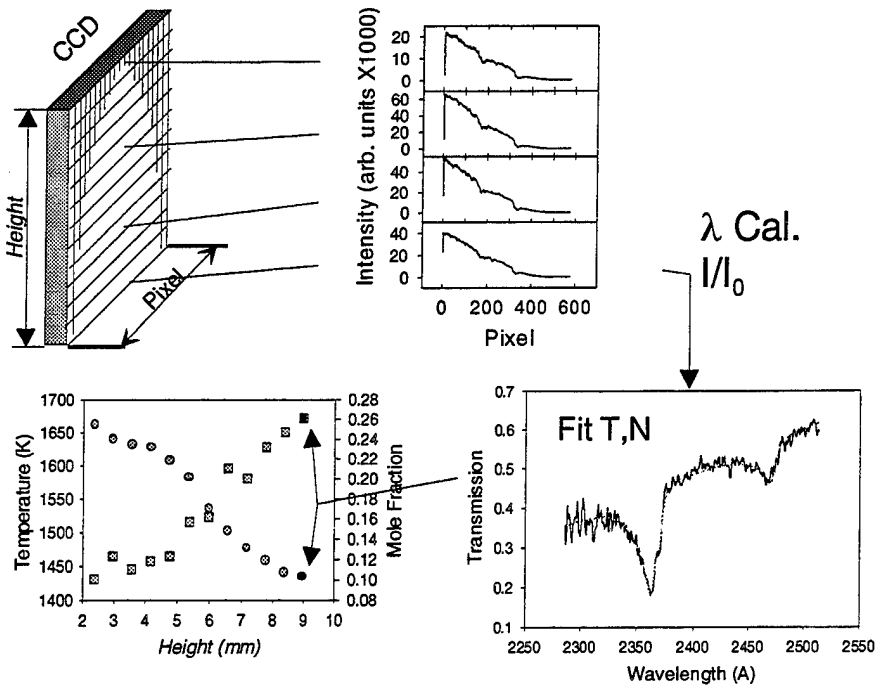

Figure 8. Data-Processing Sequence.

pen-lamp lines in the region of the high-resolution OH spectra; thus, both the wavelength offset and the wavelength per channel were allowed to vary. The fitting program convolutes the generated ideal spectra with an instrument function to account for the finite resolution of the experiment. This instrument function is determined from the FWHM of the spectral peaks collected from the pen lamp with the assumption that the physical line widths are small compared to the instrumental resolution.

The JA2 and XM39 propellant samples are solid cylinders with diameters varying between 6 and 11 mm, depending on the species being investigated. Smaller diameter samples were used for NO absorption as the concentration, and, therefore, absorption of NO, in general, is relatively high compared to OH in the same samples. Smaller diameter samples also reduced the effect of the background absorption in this region. Since the sample diameter is larger than the ignition laser beam, the top of the propellant was shaved into a cone to provide a closer match with the ignition beam area. This step seems to produce a flatter burning surface. For the OH species, a larger sample was chosen to increase the absolute absorption.

Each burn was recorded with a standard VHS video recorder and CCD camera. The recording was used to pinpoint the height of each spectrum. The exact video frame in which the data were collected is determined by a scheme in which the data frame number is recorded on the video.

3. Results

XM39 was the first propellant studied. As the amount of OH expected in the flame region of this propellant is quite low, the NO dark zone species was studied exclusively. Frames from the video recording of the XM39 combustion is shown in Figures 1 and 2. These two frames bracket the absorption light pulse. It is quite clear from these pictures that there are large changes in the combustion process that occur on a time scale less than 33 ms. The results of the present work compared to other works are shown in Figures 9 and 10 and summarized in Table 1. There appears to be reasonable agreement for the temperature of the dark zone, considering the different pressure conditions. The concentration measurements, on the other hand, show large differences. As XM39 will not self-deflagrate in N_2 at atmospheric pressure, differences are likely when comparing data taken in air with data taken in N_2. Dark zone temperatures are generally higher, and NO concentrations lower, for the self-deflagration in air; a trend consistent with oxygen participation in the combustion process. Another major contributor to the large differences in concentration is due to the problems that arise from the unsteady nature of the dark zone of LOVA propellants (i.e., flame attachment problems observed in prior work and also described in some detail by Ulas, Lu, and Kuo [1]). The snapshot absorption technique would be very useful in investigating such unstable combustion conditions. The response of a propellant to pressure perturbations is defined [12] as

$$R_p = \frac{m'}{\overline{m}} \Big/ \frac{p'}{\overline{p}}, \tag{3}$$

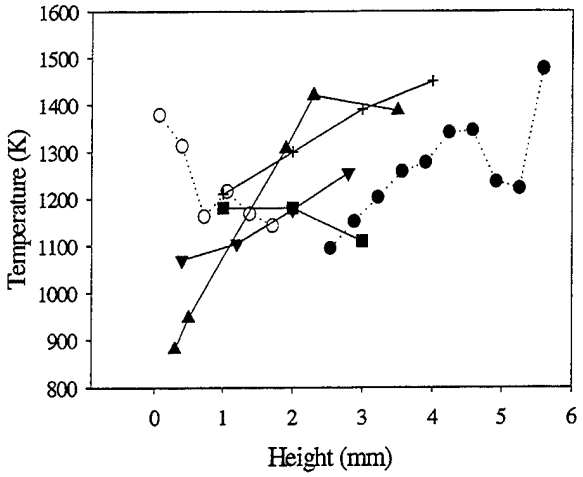

Figure 9. Dark Zone Temperatures for XM39 (● and ○ = Present Work; ■ = Teague, Singh, and Vanderhoff [3]; ▼ = Ulas, Lu, and Kuo [1]; ▲ = Mallery and Thynell [7]; ✚ = Parr and Hanson-Parr [6]).

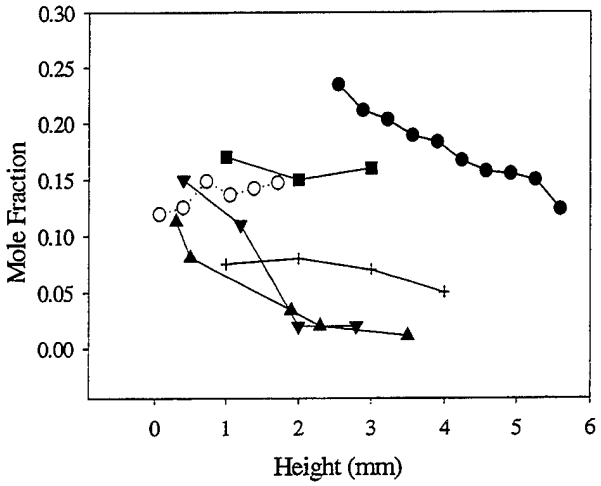

Figure 10. Concentration of NO in the Dark Zone of XM39 (● and ○ = Present Work; ■ = Teague, Singh, and Vanderhoff [3]; ▼ = Ulas, Lu, and Kuo [2]; ▲ = Mallery and Thynell [7]; ✚ = Parr and Hanson-Parr [6]).

where m and p are mass burning rate and pressure; primes and overbars indicate instantaneous and average components, respectively. For RDX (the major component of XM39), the response was maximum at 1 atm, with a value of 1.25. The frequency at maximum response was calculated to be 1.8 Hz, with a strong pressure dependence. The current readout rate of 100 kHz

Table 1. Experimental Conditions for the Data Reported in Figures 9–12

Investigator	Propellant	Spectroscopic Technique	Pressure (MPa)	Self-Deflagration
Present Work	XM39	Absorption	1.20	N_2
Teague, Singh, and Vanderhoff [3]	XM39	Absorption	1.20	N_2
Ulas, Lu, and Kuo [1]	XM39	Absorption	1.69	N_2
Mallery and Thynell [7]	XM39	Fourier-Transform Infrared (FTIR)	2.20	N_2
Parr and Hanson-Parr [6]	XM39	PLIF/Absorption	0.10	Air
Present Work	JA-2	Absorption	1.6	N_2
Vanderhoff, Teague, and Kotlar [4]	JA-2	Absorption	1.6	N_2
Lu, Freyman, and Kuo [5]	JA-2	Absorption	1.6	N_2

Note: PLIF = planar laser-induced flourescence.

effectively restricts the snapshot frequency to approximately 8 Hz for 10 simultaneous spectra. Newer cameras with readout rates of 1 MHz would increase the data collection frequency by a factor of 3–4. Assuming the response frequency of XM39 is dominated by the effect of RDX, sufficient temporal resolution exists in the current system for real-time, low-pressure (<2 atm) measurements. The current spatial resolution of 0.33 mm was a consequence of S/N considerations balanced against the need for spatial range. Increasing the spatial resolution while keeping the same S/N can be accomplished by higher lamp output or lower spatial range requirements. For the current system, resolutions below 0.1 mm would produce an unacceptable S/N.

The results for the JA-2 propellant are shown in Figures 11 and 12 and also summarized in Table 1. Both temperature and concentration data are in good agreement with data from Vanderhoff, teague, and Kotlar [4] and Lu, Freyman, and Kuo0 [5], who, like the current work, performed absorption spectroscopy at a nitrogen pressure of 1.6 MPa.

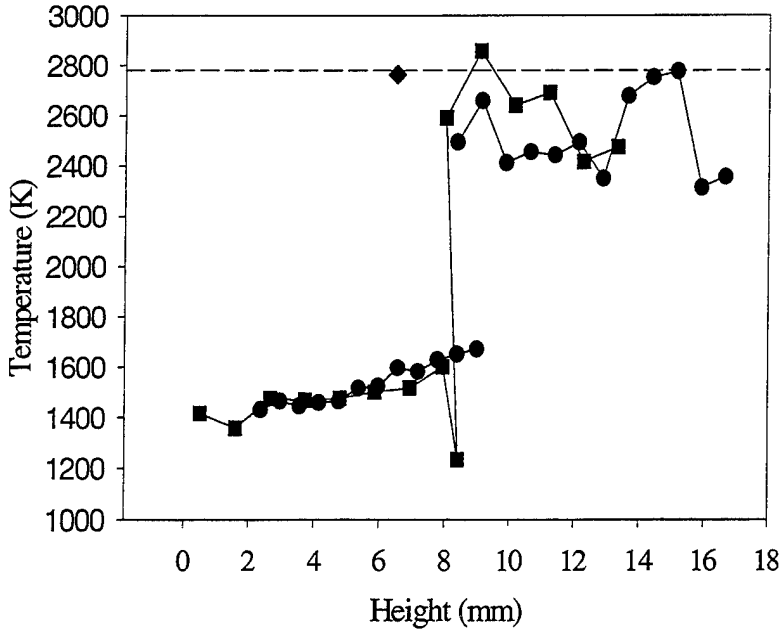

Figure 11. JA2 Temperatures in the Dark Zone and Flame (● = Present Work; ■ = Vanderhoff, Teague, and Kotlar [4]; ◆ = Lu, Freyman, and Kuo [5]; - - - = Adiabatic).

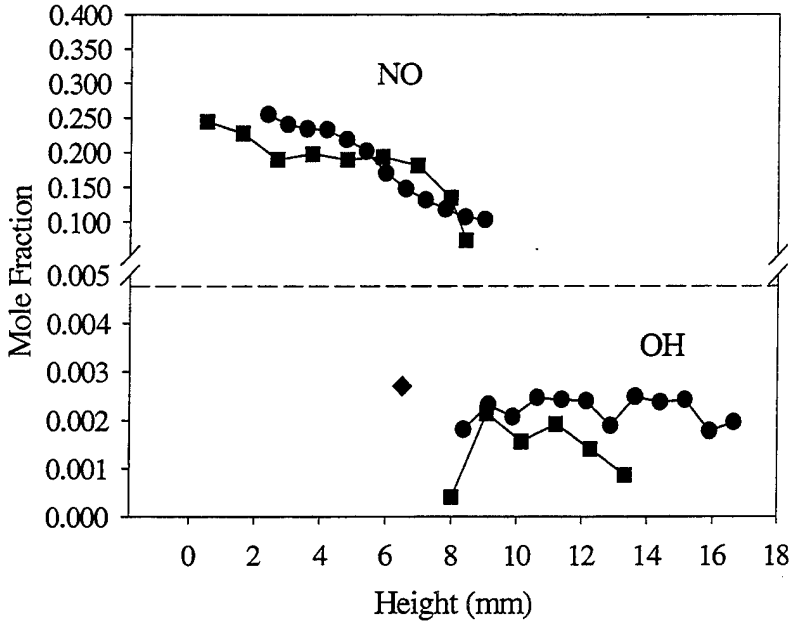

Figure 12. Concentration of NO (Upper Points) and OH (Lower Points) for JA2 (● = Present Work; ■ = Vanderhoff, Teague, and Kotlar [4]; ◆ = Lu, Freyman, and Kuo [5]; - - - = Adiabatic).

4. Summary

Modifications to the absorption experiment allowing simultaneous collection of multiple absorption spectra on a millisecond time scale have been described. The dark zone NO and luminous flame OH concentrations, as well as temperatures for XM39 and JA2, provide evidence of the practical application of this pulse absorption spectroscopy technique. The larger variation in both temperature and mole fraction of NO in XM39 is attributable to the unsteady temporal nature of this propellant at moderate pressures. JA2, on the other hand, is a much better behaved propellant in relation to the consistency of the combustion process. In this case, the agreement is much better. This snapshot absorption experiment can be used to investigate propellant combustion processes on a much finer time scale.

INTENTIONALLY LEFT BLANK.

5. References

1. Ulas, A., Y. C. Lu, and K. K. Kuo. "Determination of Temperature and OH Concentration Profiles of RDX/CAB Pseudo Propellant Using UV/Visible Absorption Spectroscopy." *Challenges in Propellant and Combustion, 100 Years After Nobel*, p. 885, K. K. Kuo (editor), Begell House, New York, NY, 1997.

2. Vanderhoff, J. A., and A. J. Kotlar. "Simultaneous Determination of Temperature and OH Concentrations in a Solid Propellant Flame." 23rd Symposium on Combustion, The Combustion Institute, p. 1339, 1990.

3. Teague, M. W., G. Singh, and J. A. Vanderhoff. "Spectral Studies of Solid Propellant Combustion IV: Absorption and Burn Rate Results for M9, XM39, and M10 Propellants." ARL-TR-180, U.S. Army Research Laboratory, Aberdeen Proving Ground, MD, 1993.

4. Vanderhoff, J. A., M. W. Teague, and A. J. Kotlar. "Determination of Temperature and NO Concentrations Through the Dark Zone of Solid-Propellant Flames." 24th Symposium on Combustion, The Combustion Institute, p. 1915, 1992.

5. Lu, Y. C., T. Freyman, and K. K. Kuo. "Measurement of Temperatures and OH Concentrations of Solid Propellant Flames Using Absorption Spectroscopy." *Proceedings of the 31st JANNAF Subcommittee Meeting*, CPIA Publication No. 620, p. 277, 1994.

6. Parr, T., and D. Hanson-Par. "Solid Propellant Flame Structure." *Decomposition, Combustion, and Detonation Chemistry of Energetic Materials*, vol. 418, p. 207, T. B. Brill, T. P. Russel, W. C. Tao, and R. B. Wardle (editors), Material Research Society, Pittsburgh, PA, 1995.

7. Mallery, C. F., and S. T. Thynell. "Species and Temperature Profiles of Propellant Flames Obtained From FTIR Absorption Spectroscopy." *Proceedings of the 31st JANNAF Subcommittee Meeting*, CPIA Publication No. 620, p. 219, 1994.

8. Homan, B. E., M. A. Miller, and J. A. Vanderhoff. "Absorption Diagnostics and Modeling Investigations of RDX Flames." *Combustion and Flame*, 1998.

9. Beck, G. "Simple Pulse Generator for Pulsing Xenon Arcs With High Repetition Rate." *Review of Science Instrumentation*, vol. 45, no. 2, p. 318, 1974.

10. Smit, K. J. "Ultraviolet and Visible Absorption Spectroscopy of Some Energetic Molecules in the Solid State." *Journal of Energetic Materials*, vol. 9, p. 81, 1991.

11. Vanderhoff, J. A., and A. J. Kotlar. "Improving Spectral Fits of Absorption Data Taken With an Array Detector: Wavelength Linearization." BRL-MR-3866, U.S. Army Ballistic Research Laboratory, Aberdeen Proving Ground, MD, 1990.

12. Beckstead, M. W., and W. W. Erikson. "Combustion Instability of Solid Monopropellant." *Proceedings of the 33rd JANNAF Subcommittee Meeting*, CPIA Publication No. 653, p. 145–157, 1996.

NO. OF COPIES ORGANIZATION

2 DEFENSE TECHNICAL INFORMATION CENTER
DTIC DDA
8725 JOHN J KINGMAN RD
STE 0944
FT BELVOIR VA 22060-6218

1 HQDA
DAMO FDQ
D SCHMIDT
400 ARMY PENTAGON
WASHINGTON DC 20310-0460

1 OSD
OUSD(A&T)/ODDDR&E(R)
R J TREW
THE PENTAGON
WASHINGTON DC 20301-7100

1 DPTY CG FOR RDA
US ARMY MATERIEL CMD
AMCRDA
5001 EISENHOWER AVE
ALEXANDRIA VA 22333-0001

1 INST FOR ADVNCD TCHNLGY
THE UNIV OF TEXAS AT AUSTIN
PO BOX 202797
AUSTIN TX 78720-2797

1 DARPA
B KASPAR
3701 N FAIRFAX DR
ARLINGTON VA 22203-1714

1 NAVAL SURFACE WARFARE CTR
CODE B07 J PENNELLA
17320 DAHLGREN RD
BLDG 1470 RM 1101
DAHLGREN VA 22448-5100

1 US MILITARY ACADEMY
MATH SCI CTR OF EXCELLENCE
DEPT OF MATHEMATICAL SCI
MADN MATH
THAYER HALL
WEST POINT NY 10996-1786

NO. OF COPIES ORGANIZATION

1 DIRECTOR
US ARMY RESEARCH LAB
AMSRL DD
J J ROCCHIO
2800 POWDER MILL RD
ADELPHI MD 20783-1197

1 DIRECTOR
US ARMY RESEARCH LAB
AMSRL CS AS (RECORDS MGMT)
2800 POWDER MILL RD
ADELPHI MD 20783-1145

3 DIRECTOR
US ARMY RESEARCH LAB
AMSRL CI LL
2800 POWDER MILL RD
ADELPHI MD 20783-1145

ABERDEEN PROVING GROUND

4 DIR USARL
AMSRL CI LP (BLDG 305)

NO. OF COPIES	ORGANIZATION
	ABERDEEN PROVING GROUND
34	DIR USARL
	AMSRL WM B
	A W HORST
	AMSRL WM BD
	B E FORCH
	W R ANDERSON
	R A BEYER
	S W BUNTE
	C F CHABALOWSKI
	S COLEMAN
	A COHEN
	R DANIEL
	R A FIFER
	B E HOMAN (10 CPS)
	A JUHASZ
	A J KOTLAR
	K L MCNESBY
	M MCQUAID
	M S MILLER
	A W MIZIOLEK
	J B MORRIS
	J E NEWBERRY
	R A PESCE-RODRIGUEZ
	P REEVES
	B M RICE
	R C SAUSA
	M A SCHROEDER
	J A VANDERHOFF

REPORT DOCUMENTATION PAGE

Form Approved
OMB No. 0704-0188

1. AGENCY USE ONLY *(Leave blank)*	2. REPORT DATE	3. REPORT TYPE AND DATES COVERED
	October 1999	Final, August 1996 - 1998

4. TITLE AND SUBTITLE
Spatially Resolved Combustion Species and Temperatures of Solid Propellant Flames Using Snapshot Spectroscopy

5. FUNDING NUMBERS
1L161102AH43

6. AUTHOR(S)
Barrie E. Homan and John A. Vanderhoff

7. PERFORMING ORGANIZATION NAME(S) AND ADDRESS(ES)
U.S. Army Research Laboratory
ATTN: AMSRL-WM-BD
Aberdeen Proving Ground, MD 21005-5066

8. PERFORMING ORGANIZATION REPORT NUMBER
ARL-TR-2060

9. SPONSORING/MONITORING AGENCY NAMES(S) AND ADDRESS(ES)

10.SPONSORING/MONITORING AGENCY REPORT NUMBER

11. SUPPLEMENTARY NOTES

12a. DISTRIBUTION/AVAILABILITY STATEMENT
Approved for public release; distribution is unlimited.

12b. DISTRIBUTION CODE

13. ABSTRACT *(Maximum 200 words)*

Experimental improvements have been made in the ultraviolet (UV)-visible absorption spectroscopy technique applied to propellant flame diagnostics. The two-dimensional (2-D) feature of an intensified charge-coupled device (ICCD) detector was used to simultaneously record multiple, spatially distinct absorption spectra over a region of 0.35 cm. Temporal resolution has been increased to 1 ms by pulsing a simmering xenon arc lamp. The resulting increase in the light intensity by 30 to 70 times over the nonpulsed output provides the necessary light flux to achieve single-pulse, multiple absorption spectra. Species with low concentrations can be measured with the inclusion of multiple-pass optics to increase the effective path length through the combustion region. Due to broadband UV-visible absorption observed in propellant flame spectra, only 20% of the incident light is typically transmitted. However, inclusion of a calibrated neutral density filter during the measurement of the incident intensity (I_0) allows the dynamic range of the detector to be effectively increased by a factor of 5. With these improvements, temperature and OH and NO concentration maps, with 1-ms temporal resolution, have been determined for two different propellant flames.

14. SUBJECT TERMS
propellant, combustion, snapshot absorption spectroscopy

15. NUMBER OF PAGES
25

16. PRICE CODE

17. SECURITY CLASSIFICATION OF REPORT	18. SECURITY CLASSIFICATION OF THIS PAGE	19. SECURITY CLASSIFICATION OF ABSTRACT	20. LIMITATION OF ABSTRACT
UNCLASSIFIED	UNCLASSIFIED	UNCLASSIFIED	UL

INTENTIONALLY LEFT BLANK.

USER EVALUATION SHEET/CHANGE OF ADDRESS

This Laboratory undertakes a continuing effort to improve the quality of the reports it publishes. Your comments/answers to the items/questions below will aid us in our efforts.

1. ARL Report Number/Author ARL-TR-2060 (Homan) Date of Report October 1999

2. Date Report Received _____

3. Does this report satisfy a need? (Comment on purpose, related project, or other area of interest for which the report will be used.) _____

4. Specifically, how is the report being used? (Information source, design data, procedure, source of ideas, etc.) _____

5. Has the information in this report led to any quantitative savings as far as man-hours or dollars saved, operating costs avoided, or efficiencies achieved, etc? If so, please elaborate. _____

6. General Comments. What do you think should be changed to improve future reports? (Indicate changes to organization, technical content, format, etc.) _____

CURRENT ADDRESS

_____
Organization

_____
Name E-mail Name

_____
Street or P.O. Box No.

_____
City, State, Zip Code

7. If indicating a Change of Address or Address Correction, please provide the Current or Correct address above and the Old or Incorrect address below.

OLD ADDRESS

_____
Organization

_____
Name

_____
Street or P.O. Box No.

_____
City, State, Zip Code

(Remove this sheet, fold as indicated, tape closed, and mail.)

(DO NOT STAPLE)